Detail-enhanced Multi-scale Exposure Fusion in YUV Color Space

Qiantong Wang, Weihai Chen*, Xingming Wu, and Zhengguo Li*

***Abstract*—It is recognized that existing multi-scale exposure fusion algorithms can be improved using edge-preserving smoothing techniques. However, the complexity of edge-preserving smoothing based multi-scale exposure fusion is an issue for mobile devices. In this paper, a simpler multi-scale exposure fusion algorithm is designed in YUV color space. The proposed algorithm can preserve details in the brightest and darkest regions of a high dynamic range (HDR) scene as well as the edge-preserving smoothing based multi-scale exposure fusion algorithm while avoiding color distortion from appearing in the fused image. The complexity of the proposed algorithm is about half of the edge-preserving smoothing based multi-scale exposure fusion algorithm. The proposed algorithm is thus friendlier to the smartphones than the edge-preserving smoothing based multi-scale exposure fusion algorithm. In addition, a simple detail-enhancement component is proposed to enhance fine details of fused images. Experimental results show that the proposed component can be adopted to produce an enhanced image with visibly enhanced fine details and a higher MEF-SSIM value. This is impossible for existing detail enhancement components. Clearly, the component is attractive for PC based applications.**

***Index Terms*—High dynamic range, Exposure fusion, Image pyramid, Multi-scale fusion, Detail enhancement.**

I. Introduction

The dynamic range of an image captured by a current imaging device can be much smaller than that of the real scene. A single exposure with a fixed exposure time inevitably results in the loss of the dynamic range. High dynamic range (HDR) imaging [1] recovers information from multiple differently exposed images of the same HDR scene. However, current display devices do not support displaying HDR images. Thus, an HDR image needs to be converted into a low dynamic range (LDR) image by tone mapping [2]-[5]. Multi-exposure fusion simplifies the pipeline and is not restricted by the lighting condition and devices. As an efficient approach to generate a high quality image, many multi-scale exposure fusion algorithms [6]-[11] have been developed since Tom et al. proposed a multi-scale exposure fusion algorithm in [12].

This work has been supported by National Nature Science Foundation of China under the research project 61620106012, 61573048, 61603020, and by the International Scientific and Technological Cooperation Projects of China under Grant No.2015DFG12650.

Qiantong Wang is with the School of Automation Science and Electrical Engineering, Beihang University, Beijing, China 100191. (e-mail: nwpuwqt@gmail.com).

Weihai Chen and Xingming Wu are with the School of Automation Science and Electrical Engineering, Beihang University, Beijing, China 100191. (e-mail: whchen@buaa.edu.cn and xmwubuaa@163.com).

Zhengguo Li is with Robotics Department, Institute for Infocomm Research, Singapore 138632. (email: ezgli@i2r.a-star.edu.sg).

*(Corresponding author: Weihai Chen and Zhengguo Li.)

Different from the HDR imaging, preserving global consistency and contrast is an important issue for multi-exposure image fusion [13]. Tom et al. proposed a classical fusion algorithm based on an image pyramid [14] as shown in Fig. 1. The weighting maps of the LDR images are constructed by taking contrast, saturation, and exposedness into consideration. It was found in [12] that naively fusing images results in inconsistency in results, especially at the border of different parts of an image. Smoothing the weighting maps is a possible way to settle this problem. But the Gaussian smoothing filter brings halo artifacts. To address such a problem, the algorithm in [12] is carried out in a multi-resolution approach. The experimental results in [15] indicate that the algorithm in [12] was the best from the MEF-SSIM point of view. However, details in the brightest/darkest regions cannot be preserved well by the algorithm in [12] as shown in Fig.2(m). Intuitively, edge-aware smoothing techniques such as [16]-[19] can be adopted to improve the Gaussian pyramid in [12]. However, the experimental results in [12] indicate that cross-bilateral filter [16] could not work well since it is difficult to find a proper guide image. Li et al. [20] proposed an interesting two-scale fusion algorithm which decomposes the LDR image into a detail layer and a base layer. In the fusion process, a guided image filter (GIF) is employed to smooth the weighting maps. Unfortunately, the algorithm in [20] suffers from halo artifacts. Recently, two novel edge-preserving smoothing techniques based multi-scale exposure fusion algorithms were proposed in [21] and [22] by introducing the weighted GIF in [18] and the gradient-domain GIF in [19], respectively. The experimental results in [23] show that the algorithm in [22] is the best one from the MEF-SSIM point of view [15]. It is recognized that edge-preserving smoothing techniques can indeed be adopted to improve existing multi-scale exposure fusion. On the other hand, the complexity of the algorithms in [21] and [22] is an issue for mobile devices. Because of the extra optimization with GGIF and WGIF, time consuming of these algorithms in [22] and [21] is about twice of that in [12], though the asymptotic complexity of these three algorithms are linear $O(N)$. There are more and more smartphones and the HDR mode is included in the smartphones. It is necessary to reduce their complexity while maintaining or improving the quality of fused images. In addition, these two algorithms could reduce color saturation of fused images as shown in Figs. 2(i) and 2(j). Both of them operate in the RGB color space. In RGB color space, R, G and B are closely related to each other [24]. In the fusion process, it is highly possible that the correlation is affected and the ratio is changed. Finally, there exists color distortion in the result compared with the real scene. To reduce

the three-channel correlation, we choose to convert the RGB to YUV. Y channel is the luminance component, while the color information is stored in U and V channels. The contrast is an important measure for an image and it is computed by applying a Laplacian filter to the Y channel of each image [12]. A natural question is that "is it possible to design a multi-scale exposure fusion algorithm in the YUV domain"? One objective of this paper is to provide an answer to this question.

Even though the multi-scale exposure fusion can be applied to preserve the global contrast better than existing single scale exposure fusion algorithms [25]-[27], the loss of detail in the process of decomposition and reconstruction is an issue for the multi-scale exposure fusion. It is thus necessary to develop a detail extraction component for the multi-scale exposure fusion, especially for those PC based applications. To compensate for the loss of detail information, Li et al. proposed a detail enhancement algorithm in [28] by using quadratic optimization. A vector field is first generated from the LDR images and the details are then extracted from the vector field and finally added to an intermediate fused image by the algorithm in [12]. It was found in [21] that there are two possible issues for the detail enhancement component in [28]. One is on the generation of the vector field and the other is on the complicated algorithm to solve the global optimization problem [3]. The concept of structure tensor [29] was adopted in [21] to improve the vector field. A fast separate approach was provided in [21] to solve the quadratic optimization problem. Based on an observation that fine details in the darkest and brightest regions of an HDR scene are respectively included in the brightest and darkest images, intelligent detail enhancement algorithms were introduced in [28] and [30]. Compared with the algorithm in [21], the complexity on the generation of vector field in [28] and [30] is much easier. On the other hand, two quadratic optimization problems are solved in [28] and [30] while only one optimization problem is solved in [21]. This indicates that the complexity of existing detail enhancement [21], [28] and [30] algorithms is still an issue. Furthermore, it was shown in [21], [28] and [30] that the MEF-SSIM values are usually reduced if visible fine details are added to intermediate fused images. This is also demonstrated by experimental results in [15]. A natural question is "Is it possible to design a simpler detail-enhanced component to improve the MEF-SSIM values when visible fine details are added to the intermediate fused images?" The other objective of this paper is to provide an answer to this question.

In this paper, we first proposed a novel multi-scale exposure fusion algorithm in the YUV color space instead of the RGB color space. The proposed algorithm is inspired by the single-scale exposure fusion algorithm in [25]. Theoretical analysis of the multi-scale exposure fusion algorithm [12] was firstly provided and a nice single-scale exposure fusion algorithm was then proposed in [25]. Although the algorithm in [25] could introduce halo artifacts, it indeed provides a novel way to simplify the existing multi-scale exposure fusion algorithm. By analyzing the algorithms in [22] and [25], it is observed that a nice approximation on edge-preserving smoothing is also provided in [25]. The proposed algorithm is designed on top

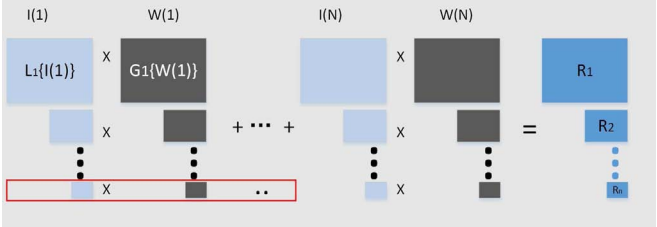

Fig. 1: General pipeline of multi-scale exposure fusion. I(1)-I(N) are N LDR images. W(1)-W(N) are weighting maps. In the process, LDR images are decomposed into the Laplacian pyramids, and the weighting maps are decomposed into the Gaussian pyramids. '$\times$' is dot product. R_1-R_n are layers of the result Laplacian pyramid.

of such an observation. Compared with the algorithms based on the WGIF in [21] and GGIF in [22], our algorithm gets competitive results by employing an approximation algorithm to optimize the highest layer of the pyramid. The number of the pyramid layers is same as that in [22] and [21]. There are two options: 1) the approximation algorithm is only performed on images with exposure times which are smaller than the middle one; and 2) the approximation algorithm is conducted on all the images. The former is selected in this paper because both the MEF-SSIM and the global contrast are improved by the former. Experimental results show that the proposed multi-scale exposure fusion algorithm can be adopted to obtain comparable or even better results than the state-of-the-art exposure fusion algorithms in [22]. Meanwhile, the proposed algorithm is much simpler than the algorithms in [21] and [22]. It is thus friendlier to the smartphones.

Same as the existing multi-scale exposure fusion algorithms, the proposed multi-scale exposure fusion could suffer from losing details. To make up for the lost detail information in the fusion process, we proposed a novel and simple vector field construction algorithm, which is inspired by the algorithm in [29] and [30]. By solving a global optimization problem with new parameter settings, visible fine details are extracted from the vector field. The final detail-enhanced image is generated by adding the detail layer to an intermediate image produced by the proposed multi-scale exposure fusion algorithm. Experimental results indicate that the proposed detail enhancement algorithm outperforms the algorithms in [21], [28] and [30] in the sense that the MEF-SSIM of the detail-enhanced image is improved in presence of visible enhanced fine details. This is impossible for the detail enhancement algorithms in [21], [28] and [30]. The proposed detail-enhancement component is thus attractive for PC based applications. Overall, two major contributions of this paper are: 1) a simpler multi-scale exposure fusion algorithm which can achieve comparable or even better results than the algorithm in [22]; and 2) a simpler detail enhancement component which can produce an image with visibly enhanced fine details and a higher MEF-SSIM.

The remainder of this paper is organized as follows. A novel multi-scale fusion algorithm in YUV color space and ROI exposure fusion are introduced in section II. Detail enhancement of exposure fusion image is studied in section

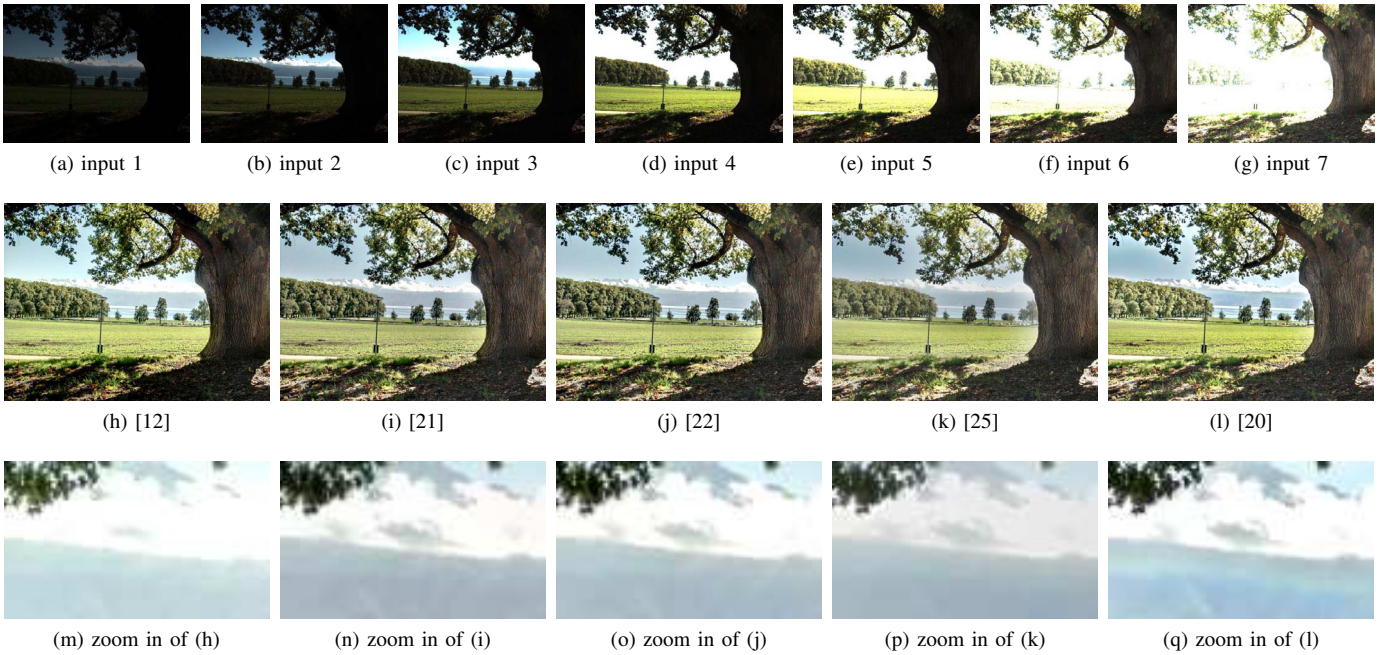

(a) input 1 (b) input 2 (c) input 3 (d) input 4 (e) input 5 (f) input 6 (g) input 7

(h) [12] (i) [21] (j) [22] (k) [25] (l) [20]

(m) zoom in of (h) (n) zoom in of (i) (o) zoom in of (j) (p) zoom in of (k) (q) zoom in of (l)

Fig. 2: Sample results of several different exposure fusion algorithms. Detail loss in bright area of [12] is main issue of this algorithm on LDR image set "treeunil". The state-of-the-art fusion algorithms [21] and [22] suffer from color distortion. The fused image by [25] looks flat. Halo artifacts exist in result of [20]. Image courtesy of Laurence Meylan.

III. Conclusion remarks are given in the last section.

II. Multi-scale exposure fusion in YUV Color Space

In this section, we introduce a simpler multi-scale exposure fusion algorithm in the YUV color space.

A. Construction of weighting map

Construction of weighting map is carried out in YUV color space, which takes human perception feature into consideration. First, normalize and convert RGB into YUV color space. Similar to [12], three measurements, contrast, saturation and exposure, are adopted to compute the weighting maps of the LDR images. They are denoted by C, S and E, respectively. The difference is that in the proposed algorithm, weighting measurements are computed in the YUV color space while RGB color space in [12]. Generally, in an under/over-exposed region, edges of an object are difficult to be detected. The Laplacian operator $[0,-1,0;-1,4,-1;0,-1,0]$ is adopted to calculate the contrast C. C is the absolute value of the convolution of Laplacian operator L and channel Y. Larger weights will be given to pixels at an edge.

$$C =\mid L * Y \mid \tag{1}$$

A well-exposed pixel captures color saturation well. The standard deviation within the R, G and B channel of each pixel is taken as measure S [12]. While in YUV color space, S is computed as

$$S =\mid U \mid + \mid V \mid +1 \tag{2}$$

Over-exposed and under-exposed pixels generally fail to capture key detail information genuinely. From the view of probability, the brightness of well-exposed pixels tend to be close to 0.5 [12]. Measure E is computed as follows:

$$E = e^{-\frac{(Y-\mu)^2}{2\sigma^2}} \tag{3}$$

in which Y is the normalized value of Y channel. Two parameters of the Gaussian kernel, σ and μ are set to 0.2 and 0.5, respectively [12]. To increase the SNR and to preserve the detail information in the dark areas, a quality measure $B = \overline{Y}^2$ in [31] is introduced in the proposed algorithm.

The weighting maps are yielded by [12]:

$$W_{ij,k} = C_{ij,k}^{\omega_C} \times S_{ij,k}^{\omega_S} \times E_{ij,k}^{\omega_E} \times B_k^{\omega_B} \tag{4}$$

where ij,k refers to pixel ij in the kth LDR image. ω_C, ω_S, ω_E and ω_B are weights of four quality measures, which are set to default value 1 [12]. To ensure the sum of the weights is 1 [12], the weighting maps are normalized as follows:

$$\overline{W}_{ij,k} = [\sum_{\overline{k}=1}^{N} W_{ij,\overline{k}}]^{-1} W_{ij,k} \tag{5}$$

where $\overline{W}$ are normalized weighting maps of N LDR images.

B. Multi-scale exposure fusion

In this subsection, the reasons why detail information is lost in the fusion process and why halo artifacts happens in the results are discussed. Then, we examine the possible solution to preserve the detail information and to suppress the halo artifacts. Finally, a simpler multi-scale fusion algorithm is proposed to preserve details in over-exposed and under-exposed regions well. The proposed algorithm is inspired by the algorithms in [21], [22] and [25].

In the proposed algorithm, both the weighting maps and the LDR images are decomposed into n layers as shown in Fig. 1. The value of n is given as [22]

$$n = \lfloor log_2(min(h, w)) \rfloor - 2 \tag{6}$$

in which $\lfloor x \rfloor$ returns a nearest integer less than or equal to x, with h and w representing the number of rows and columns of an image, respectively. The Gaussian pyramid is constructed as the equations (7) and (8).

$$G_{l+1} = Down(G_l \otimes G_{kernel}) \tag{7}$$

A higher layer is obtained by decimating the lower layer, which is smoothed by a Gaussian kernel G_{kernel}, with a decimation factor of 2 in the vertical and horizontal direction. The Laplacian pyramid is constructed by the information lost in the decimation process:

$$L_l = G_l - Up(G_{l+1}) \otimes G_{kernel} \tag{8}$$

$Down$ and Up represent the downsampling and upsampling, with $\otimes$ denoting convolution.

The Gaussian pyramid can be viewed as a low-passing filter. On the other hand, the Laplacian pyramid can be viewed as a band-pass filter. The layers of the Laplacian pyramid store high-frequency information. It is worth noting that the highest layer of the Laplacian pyramid is the highest layer of the Gaussian pyramid in this algorithm.

The number of the pyramid layers in [22] and the proposed algorithm is 2 less than that in [12]. For the multi-scale exposure fusion in [12], reducing the number of scales is a possible way to preserve detail information better. But simply reducing the number of layers of the pyramid is not the solution because of the consequential halo artifacts [25] and [31]. By scrutinizing the $n-th$ layer of the Gaussian pyramid in detail, we find out that, at the high layers of the weighting pyramids, the improper smoothing around the edge is the main reason why halo emerges, as shown in Fig. 3(a)-(c). For instance, the over-exposed regions along the border of the normally exposed areas tend to have higher weights, which results in the halo artifacts around the edge. The ideal solution is to eliminate the improper weighting. However, such a course is almost impossible since there is no clear line to define the boundary between the high and low weighting areas. Also, it is inappropriate to eliminate such improper weighting, since the weighting is always varying gradually, which means an edge like a cliff will introduce the serious inconsistency in lightness across the whole image (Fig. 3.(h)). Thus, it seems that the possible solution is to smooth or spread the halo artifacts to the whole image, making it unobservable.

Basically, a Gaussian smoothing filter can be adopted at the $n-th$ level to attenuate the halo artifacts. However, in this case, as shown in Fig. 3.(m), compared with $G_n\{W(N)\}$, the smoothed $G_n\{W(N)\}$ reduce the weight of the properly-exposed area. Besides, detail information, especially in the lightest area, will be affected since over-exposed areas are assigned with higher weights (Fig. 3.(i)). The GGIF is indeed a good idea, but for same LDR images, the computational time of the algorithm in [22] is almost twice of that in [12].

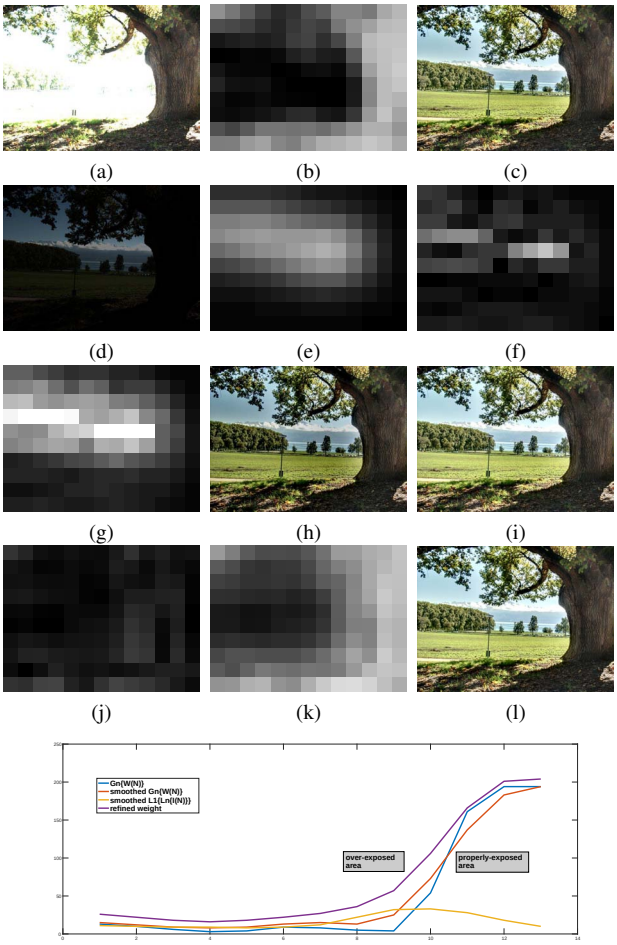

(m) Illustration of one row sampled from the weighting maps

Fig. 3: (b) is the $n-th$ layer of the weighting map of (a). It can be observed that, in the over-exposed area, weighting along the tree increases because of the smoothing in the decomposition of the weighting map of (a). This is a main reason why halo happens. (c) is the corresponding result. (e) is the $n-th$ layer of the weighting map of (d). (f) is the smoothed version of $|L_1\{L_n\{I(1)\}\}|$. (g) is the sum of (e) and (f), which has higher weight in the light area. (j) is the smoothed version of $|L_1\{L_n\{I(N)\}\}|$. (k) is the sum of (b) and (j).

We also find out that applying the edge-preserving filter at low layers is not cost-effective to suppress the halo artifacts across the whole image. The halo across the whole image mainly results from improper weighting at the high levels, which means necessary measurements should be taken at the high-level instead of the low-levels. For another, because the size of the image at the low layer is large, such a process is rather time-consuming. Though the algorithm is simplified as [31], in some cases, smoothing the weighting maps with the GGIF merely at the highest layers cannot effectively preserve the global contrast as well as [22]. Moreover, an extra guided image filter needs to be constructed in [31], which slightly increases the complexity.

Motivated by [25], [31], [32] and scrutinized the $n-th$ layer of the pyramid of weighting maps, we find out that

(a) $\bar{\sigma} = 0.5$ (b) $\bar{\sigma} = 1$ (c) $\bar{\sigma} = 3$

Fig. 4: Results of fusion algorithm adopting the Gaussian filter with different $\bar{\sigma}$'s. Image courtesy of Jacques Joffre.

the Laplacian pyramid of Y channel can be adopted to solve this problem after some reasonable pretreatment. In [25], detail information is preserved well with a single scale fusion method. In that algorithm, information from the Laplacian pyramid of LDR image is added to the smoothed weighting map. The single scale fusion algorithm in [25] was denoted by:

$$R^k = [G_{\tilde{n}}\{\overline{W}(k)\} + \alpha|L_1\{I(k)\}|]I(k), k = 1, 2, ..., N \quad (9)$$

where $I(k)$ is an input LDR image. R^k is the fusion result of the $k-th$ LDR image and its weighting map. $G_{\tilde{n}}\{\overline{W}(k)\}$ represents the $\tilde{n}-th$ layer of the Gaussian pyramid of $\overline{W}(k)$. In [25], $\tilde{n}$ is the maximum number of the Gaussian pyramid. N is the total number of LDR images. $L_1\{I(k)\}$ is the first layer of the Laplacian Pyramid of the input $I(k)$. α is the coefficient of the $L_1\{I(k)\}$, which controls the magnitude of the high-frequency signal—$L_1\{I(k)\}$. The terms in the square brackets can be viewed as the weighting of $I(k)$.

It can be observed from the equation (9) that the approximation method (9) shares one feature with the WGIF [18] and the GGIF [19], i.e., all of them intend to preserve edges while smoothing. The approximation method (9) is simpler than both the WGIF and the GGIF. Based on the above observation and analysis, a new multi-scale exposure fusion algorithm is designed as below. An basic approximation formulation at the $n-th$ layer is derived by substituting $\overline{W}(k)$ and $I(k)$ in equation (9) with $G_n\{\overline{W}(k)\}$ and $L_n\{I(k)\}$:

$$R_n^k = [G_2^{'}\{G_n\{\overline{W}(k)\}\}+\alpha|L_1\{L_n\{I(k)\}\}|]L_n\{I(k)\} \quad (10)$$

As shown in Fig.3.(m), Eq.(10) guarantees the weighting of properly exposed area is not affected by smoothing. Besides, the improper weight is smoothed to a broad area to attenuate the halo. In this way, it has similar effects as GIF based filter.

As for the rest scales, the fusion is operated as follows [12]:

$$R_l^k = G_l\{\overline{W}(k)\}L_l\{I(k)\}, l = 1, 2, ..., n-1 \quad (11)$$

with l denoting the level of the pyramid.

Based on the observation that the improper smoothing brings the halo artifacts, the weighting maps and the LDR images are fused by adopting the proposed algorithm at the $n-th$ layer instead of all layers [22]. First, the Gaussian smoothing filter is employed to smooth the $n-th$ layer of the weighting maps to ensure the consistency and eliminate the halo artifacts. The $G_2^{'}\{G_n\{\overline{W}(k)\}\}$ is the decomposition of the $G_n\{\overline{W}(k)\}$, in the experiment, a Gaussian smoothing filter is employed to smooth $G_n\{\overline{W}(k)\}$. Being smoothed by a Gaussian smoothing filter, for under-exposed LDR images, the weights of the properly exposed areas (light areas) around the edge decrease. This is one reason why detail information is not preserved well in the light area. For over-exposed LDR images, the weighting of the improperly exposed area (light area in the scene but over-exposed) will increase, which is another reason for the loss of detail in the light area. To address this problem, $|L_1\{L_n\{I(k)\}\}|$ is introduced to refine the weighting maps. $|L_1\{L_n\{I(k)\}\}|$ contains high-frequency information—the edge between the improperly and properly exposed areas, which can be adopted to correct the improper weighting brought by the Gaussian smoothing as shown in Fig. 3(d)-3(g).

Whereas, adding $|L_1\{L_n\{I(k)\}\}|$ directly to the smoothed weighting maps for all the LDR images is not always a good solution since the operation increases the weights of the light areas in the over-exposed LDR images as shown in Fig.3(j)-(l). To preserve the detail information in the light areas, it is supposed to increase the weights of well-exposed light areas. It is mentioned that the detail information in the light areas is well preserved in the under-exposed LDR images in [21] and [33]. Even though Eq.(10) guarantees the weighting of properly exposed area is not affected by smoothing. It has slight influence on the improperly-exposed area. Therefore, Eq.(10) is only adopted to optimize the weighting maps of the under-exposed images. For over-exposed images, the basic Gaussian smoothing filter is adopted to smooth the $n-th$ layer of the weighting maps. To get more consistent brightness distribution, the same Gaussian filter is used to smooth the $|L_1\{L_n\{I(k)\}\}|$. In this course, the smoothed $|L_1\{L_n\{I(k)\}\}|$ is added to the weighting maps, which properly increases the weights of the well-exposed areas in the under-exposed images as shown in Fig. 3(d)-3(g). After normalization, the light areas in the under-exposed images will be assigned with higher weighting, which is conducive for preserving the detail information in the light area.

The standard variation $\overline{\sigma}$ and width $\overline{w}$ of the Gaussian kernel used to smooth the $G_n\{\overline{W}(k)\}$ and $|L_1\{L_n\{I(k)\}\}|$ are set to 1 and 3. Parameter α controls the intensity of high-frequency signal which represents edges. In the experiment, α is set to 1.5. Increasing the α in the certain range is helpful for preserving details, especially in the light area.

As shown in Fig. 4(a), halo artifacts exist in the fused results if standard variation $\overline{\sigma}$ is small. Fortunately, a large standard variation is conducive for suppressing halo artifacts. The Gaussian filter with a small standard variation $\overline{\sigma}$ cannot effectively smooth the $n-th$ layer, which reflects the overall brightness feature of the image. Generally, the Gaussian kernel $\overline{w}$ is 6 times of standard variation to include as much valuable information as possible. But in the experiment, it is found that the large width results in detail loss in the bright area, so the width of the Gaussian kernel $\overline{w}$ is set to 3.

The final fusion image R is generated by reconstructing the Laplacian pyramid made up by R_l. Each layer of the final

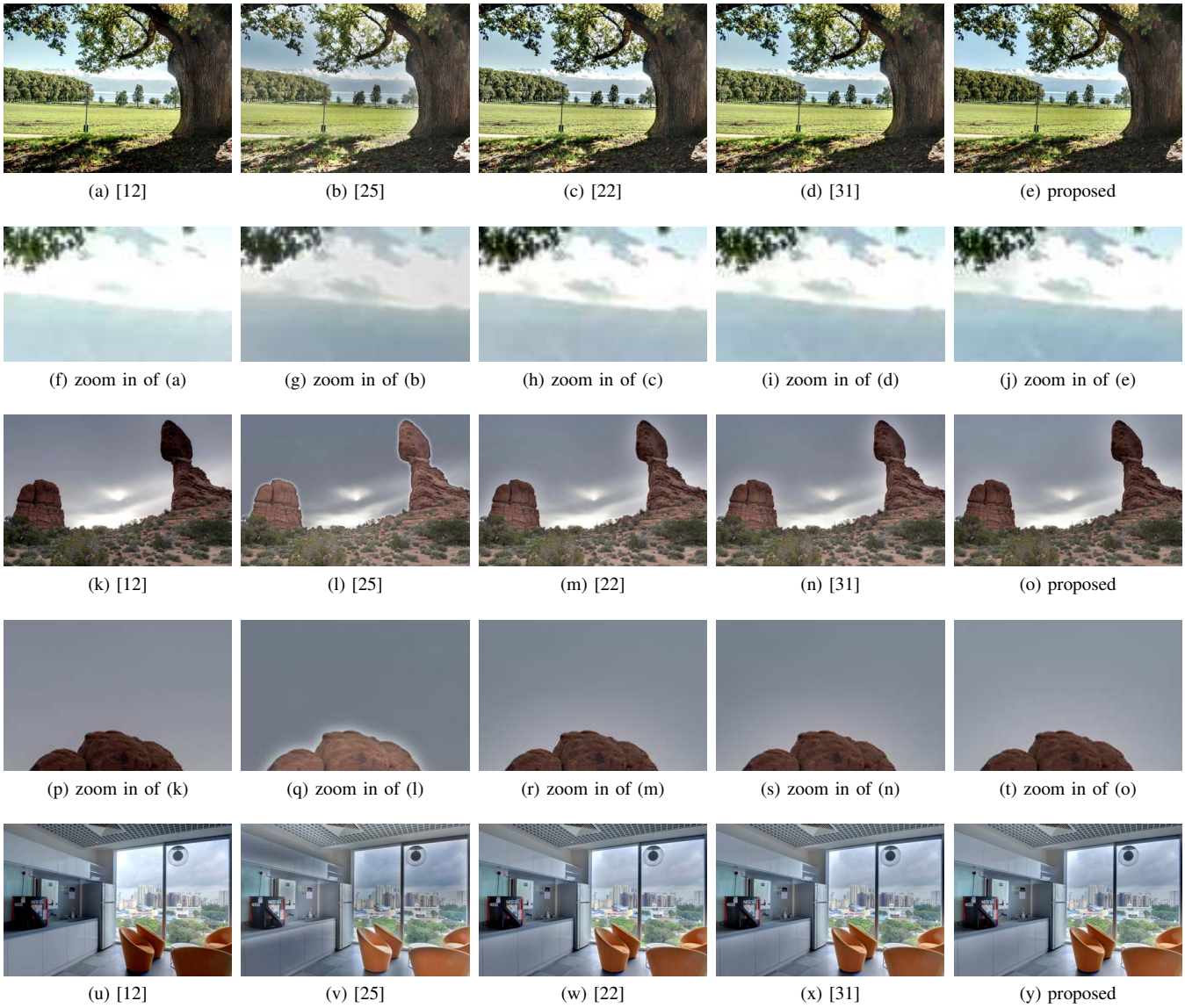

(a) [12] (b) [25] (c) [22] (d) [31] (e) proposed

(f) zoom in of (a) (g) zoom in of (b) (h) zoom in of (c) (i) zoom in of (d) (j) zoom in of (e)

(k) [12] (l) [25] (m) [22] (n) [31] (o) proposed

(p) zoom in of (k) (q) zoom in of (l) (r) zoom in of (m) (s) zoom in of (n) (t) zoom in of (o)

(u) [12] (v) [25] (w) [22] (x) [31] (y) proposed

Fig. 5: Comparison of results of proposed multi-scale fusion algorithm and several fusion algorithms [12], [22], [25] and [31].

(a) [12] (b) [25] (c) [22] (d) [31] (e) proposed

Fig. 6: Comparison of results of five fusion algorithms on one LDR image sets with noise.

Laplacian pyramid is yielded by:

$$R_l = \sum_{k=1}^{N} R_l^k, l = 1, 2, ..., n \tag{12}$$

The proposed exposure fusion is carried out in Y channel, while the Gaussian pyramid [12] based fusion algorithm is adopted in U and V channels. The reason is that the Y channel is key for the contrast and the perception. U, V channels store color information, which has limited influence on structure information. It is worth noting that the numbers of pyramid layers are same for the three channels.

In the proposed algorithm, the weighting maps are optimized with a simple addition instead of the complex guided image filter. By adopting the refined weighting when fusing the Y channels, the halo artifacts are removed effectively, with the detail information preserved well.

(a) input 1 (b) input 2 (c) input 3

(d) ω_1:ω_2:ω_3=1:1:1 (e) ω_1:ω_2:ω_3=1:2:3

(f) ω_1:ω_2:ω_3=1:3:5 (g) ω_1:ω_2:ω_3=1:4:7

(h) zoom in of (d) (i) zoom in of (e) (j) zoom in of (f) (k) zoom in of (g)

Fig. 7: Comparison of results of ROI exposure fusion. (The third input image is selected as dominant image. The normalized weights of the third weighting map in four cases are $1/3, 1/2, 5/9, 7/12$)

C. ROI exposure fusion

The proposed exposure fusion can be enhanced by incorporating the concept of region of interest (ROI). The weighting maps decide the contribution of each pixel to the final fused image. In the LDR image set, differently exposed LDR images include different well-exposed regions in one HDR scene. The LDR image in which ROI is well exposed is selected as the dominant image. Higher weights are assigned to the weighting map of this image, while relatively lower weights to the weighting maps of the others. Thus, after normalization, the ROI will be highlighted in the final fused image. Overall, the weighting map is constructed as follows:

$$W_{ij,k} = \omega_k \times C_{ij,k}^{\omega_C} \times S_{ij,k}^{\omega_S} \times E_{ij,k}^{\omega_E} \times B_k^{\omega_B} \tag{13}$$

where ω_k is the weight of the kth weighting map. $\times$ is dot product, which limits influence on the under/over-exposed area considering the weights of under/over-exposed regions are small. ROI in LDR image with larger ω_k will be highlighted in the final results.

III. Detail Enhancement of Exposure Fusion Image

In the process of pyramid decomposition and reconstruction, more details are lost as the total number of pyramid layers increases, since Gaussian low-passing filters are employed in the decomposition. However, smoothing the weighting maps is an essential role of the Gaussian filter in exposure fusion. Simply decreasing the total number of pyramid layers is not a solution considering the resultant unpleasing halo and inconsistency in result [25]. To compensate for the detail lost in the fusion process, a detail extraction, and enhancement algorithm are proposed in this section.

A. Vector field construction

The LDR images store all valuable detail information, therefore, to compensate for the lost detail information, detail must be extracted from these LDR images directly. Considering the nonlinear feature of the human visual system [34], Y channel is converted into the logarithmic domain as follows:

$$I = log_2(Y + 1) \tag{14}$$

Intuitively, detail is reflected by the variations in intensity of pixels, which can be represented by a gradient. In this algorithm, a gradient field is constructed adopting forward difference in the vertical and horizontal direction.

$$(Grad_h, Grad_v) = (I_{i+1,j} - I_{i,j}, I_{i,j+1} - I_{i,j}) \tag{15}$$

where $Grad_h$ and $Grad_v$ denote gradient in the horizontal and vertical direction.

In the under-exposed and over-exposed LDR images, the brightest and darkest regions are exposed properly, respectively. Most details of the darkest and lightest zones are captured in the darkest region of lightest LDR image and the lightest region of darkest LDR image, respectively. Furthermore, in the over-exposed and under-exposed areas, considering low SNR, a weighting function is needed to suppress the noises, as well. Two weighting functions for the darkest and brightest LDR images are constructed as the equation (16). Threshold θ_1 and θ_N are two adjustable parameters which determine the region is enhanced. Users can adjust the threshold according to their preference.

$$\begin{aligned} T_1 &= \begin{cases} Y_1 + 1, & \text{if } Y_1 < \theta_1 \\ \max\{\theta_1 + 1 - 16(Y_1 - \theta_1), 0\}. & \text{otherwise} \end{cases} \\ T_N &= \begin{cases} 256 - Y_N, & \text{if } Y_N > \theta_N \\ \max\{256 - \theta_N + 16(Y_N - \theta_N), 0\}. & \text{otherwise} \end{cases} \end{aligned} \tag{16}$$

For simplification, $T_1(p)$, $T_N(p)$, $Y_1(p)$, and $Y_N(p)$ are simplified as T_1, T_N, Y_1 and Y_N. Here $T_1(p)$ and $T_N(p)$ are weights of the gradient in the darkest and brightest LDR images, respectively. Vector fields are constructed by a weighted average of gradient field of the under/over-exposed LDR images. The vector field in the horizontal direction is constructed as follows:

$$V_h(p) = \begin{cases} \dfrac{\sum\limits_{i\in\{1,N\}} T_i(p)T_i(p_r)Grad_h(p)}{\sum\limits_{i\in\{1,N\}} T_i(p)T_i(p_r)}, & \text{if } \sum\limits_{i\in\{1,N\}} T_i{}' > 0 \\ 0. & otherwise \end{cases} \tag{17}$$

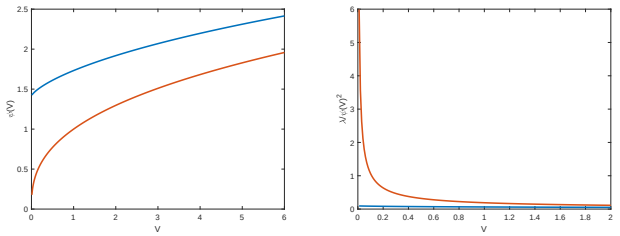

(a) (b)

Fig. 8: The red solid line and blue solid line represent curves of $\psi(V) = \sqrt{\mid V \mid^{0.75} +10^{-4}}$ and $\psi(V) = \sqrt{\mid V \mid^{0.75} +2}$. In (b), $\lambda = 0.19$ is computed by FWLS in [35].

Here, p_r is the right conjunction pixel of pixel p. $T_i^{'}$ is $T_i(p)T_i(p_r)$. A similar operation is adopted in the vertical direction. Clearly, the proposed vector field construction algorithm is much simpler than the structure tensor based algorithm in [21].

B. Detail extraction

Detail is subtracted from the vector filed by solving a quadratic optimization problem. The cost function of quadratic optimization is constructed as follows [28]:

$$\min_{L_d}\{[\|L_d\|^2 + \lambda(\|\frac{V_h - \frac{\partial L_d}{\partial x}}{\psi(V_h)}\|_2^2 + \|\frac{V_v - \frac{\partial L_d}{\partial y}}{\psi(V_v)}\|_2^2])\} \quad (18)$$

The first term is smoothing term which results in detail layer, whose value is near to 0. The second term is fidelity term which preserves the detail information. The parameter λ controls degree the vector field is smoothed. λ is set to 0.5 in the proposed algorithm while it is 0.03125 in [21]. $\psi(V_h)$ and $\psi(V_v)$ [3] and [28] are edge-aware regularization terms. The function $\psi(V)$ is defined as:

$$\psi(V) = \sqrt{\mid V \mid^{\gamma} +\varepsilon} \quad (19)$$

The exponent γ determines the sensitivity to the gradients, and ε is a constant that prevents division by zero error [3].

Different from settings in [3], [21], [28] and [33], the value of ε is set to 2 rather than 10^{-4}. Such a change is vital for the improvement of the quality of the detail-enhanced image (Fig. 8). According to the equations (18) and (19), the value of $\lambda/\psi(V)^2$, at a clear edge, is small while large at the relatively smooth area. However, a slight variation does exist in a smooth region. As a matter of fact, it is not desirable that such little variations being amplified. In [21], a large value of the $\lambda/\psi(V)^2$ is yielded in such an area, which results in unpleasing rough texture in the detail-enhanced result. To address this problem, the value of ε is set to 2. In this way, $\lambda/\psi(V)^2$ is small in the case that small variations and noises exist.

A detail-enhanced image is generated by adding the detail layer to the result of exposure fusion. Mathematically, the detail-enhanced image R^* is generated as follows:

$$R^* = R * 2^{L_d} \quad (20)$$

IV. Experimental Results

In this section, to validate the effectiveness of the proposed exposure fusion algorithm, the proposed algorithm is evaluated by testing 16 different LDR images sets from several DataSets. (Link1: http://ivc.uwaterloo.ca/database/MEF/MEF-Database.php; Link2: http://rit-mcsl.org/fairchild/HDR.html). Readers are invited to view the electronic version of the paper for better appreciation of the difference among images.

A. Evaluation of the proposed multi-scale exposure fusion

The proposed multi-scale exposure fusion algorithm and detail enhancement component are first compared with three state-of-the-art exposure fusion algorithms including [12] which was remarked as the best overall performance by [15], [22] which was remarked as the best one by [23], and [25] which is the latest single-scale fusion algorithm. A simplified GGIF based MEF algorithm [31] is also included in the experiment. The MEF-SSIM [15] is adopted as an image quality assessment metric of the experiment results. The scores are listed in Table I. It can be found that the proposed algorithm has better overall performance than that in [12] on these different LDR images sets. The computational time of the four exposure fusion algorithms are given in Table II. All of the experiments are carried out on MATLAB 2016, [intel core i7-6700, 16GB RAM]. It can be shown that the proposed algorithm can achieve the comparable MEF-SSIM to the state-of-the-art algorithm in [22] while the complexity is reduced by around 50%. Supposing that an image consists of N pixels, the asymptotic time complexity of constructing the weighting maps and image pyramids is $O(N)$. The asymptotic time complexity of the GGIF can be $O(N)$ with the box filter. Thus the overall time complexity of [22] is $O(N)$. The asymptotic time complexity of the proposed algorithm is almost $O(1)$ since the size of the $n-th$ layer is always about $8 * 8$ no matter the size of the input images. Though the overall time complexity is $O(N)$ as well, the computational time of the proposed exposure fusion algorithm is much less. Both the [22] and the proposed algorithm are on top of the algorithm in [12]. The time consumption comes from two main parts, the construction of the image pyramids and the optimization by GGIF or the proposed method. In the proposed method, the proposed filter is merely employed at the $n-th$ layer of the weighting pyramids. Also, such an algorithm is only adopted in the Y channel of part of the LDR images. While the [22] is employed on all the pyramid layers for all the LDR images. Though the [22] can also be simplified as the method in [31], it needs the extra guide image. Building up a pyramid of guided image filtering leads to extra computational time compared with the proposed algorithm. Thus, for the same LDR images, the proposed method spend almost the same time as [12], half of the time consumed by [22].

From the sample results in Fig. 5 and Fig. 6, it can be founded that the algorithm in [12] preserves the global contrast and the color saturation well while it cannot preserve the details in the darkest and brightest regions. The algorithm in [25] preserves the color saturation as well as the details in the darkest and brightest regions while it cannot preserve

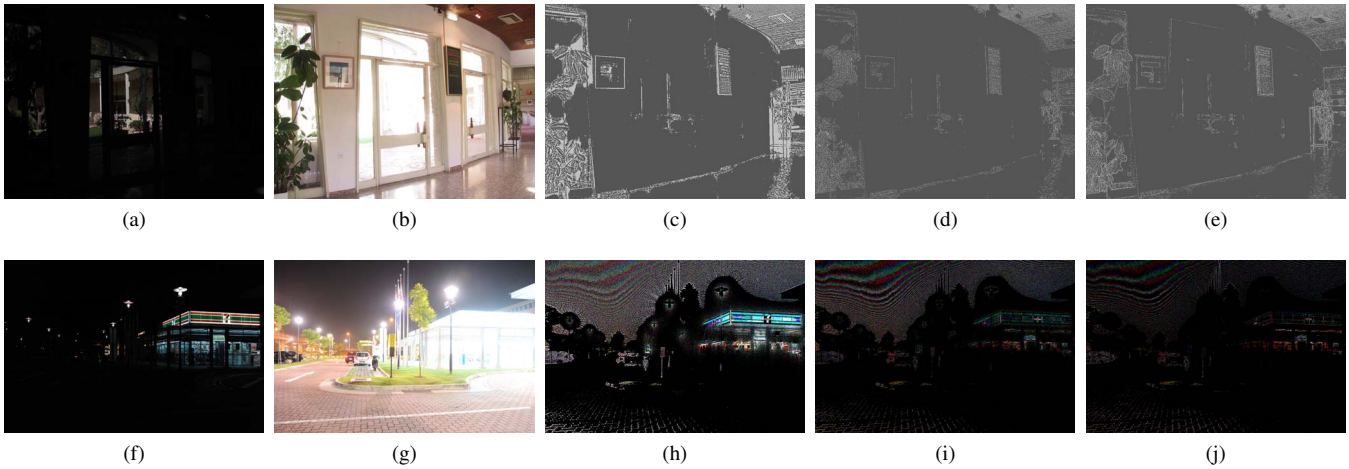

(a) (b) (c) (d) (e)

(f) (g) (h) (i) (j)

Fig. 9: Comparison of details extracted by different settings for the detail extraction component in the proposed algorithm on LDR image set "BelgiumHouse". (a) (f) and (b) (g) are the darkest and lightest LDR images. For (c)-(e) and (h)-(j) the value of γ is fixed at 0.75. (c) and (h): $\epsilon = 10^{-4}$ and $\lambda = 0.5$; (e) and (i): the recommended settings in [21]; and (d) (j): the proposed settings. Image courtesy of Dani Lischinski.

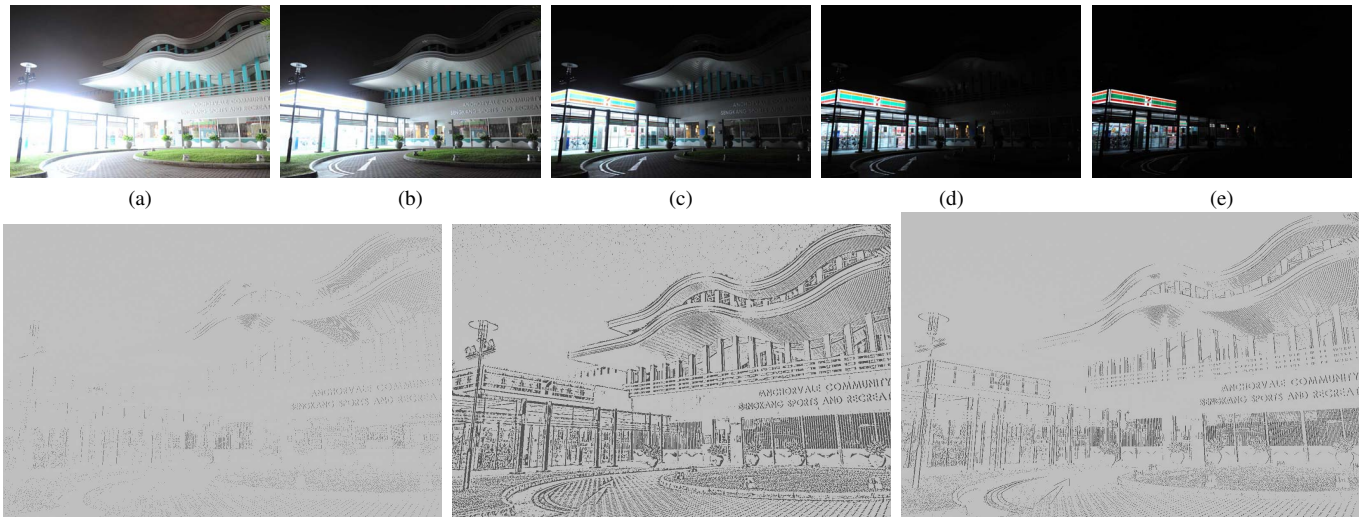

(a) (b) (c) (d) (e)

(f) (g) (h)

Fig. 10: Comparison of details extracted by different settings for the detail extraction component in [21]. The value of γ is fixed at 0.75. (a)-(e): input images; (f): the recommended settings in [21]; (g): $\epsilon = 10^{-4}$ and $\lambda = 0.5$; and (h): the proposed settings.

the global contrast. It sometimes suffers from halo artifacts as shown in Fig. 5(l) and Fig. 5(q). The algorithm in [22] can preserve the global contrast as well as the details in the brightest and darkest regions well but it reduces the color saturation. For example, grass and leaves of the set "Treeunil" tend to be gray. The proposed algorithm can preserve all the global contrast, the details in the brightest and darkest regions and the color saturation well as shown in Fig. 5(c) and Fig. 5(e). The grass and leaves tend to be green. Though the algorithm in [31] preserves the details in both light and dark areas well, it does not preserve the global contrast as well as the algorithm [22].

At the end of this subsection, the proposed ROI based exposure fusion algorithm is tested. The image set and comparison results are posted in Fig. 7. Compared with the results of exposure fusion adopting equivalent weighting for LDR images, the result of the ROI exposure fusion preserves facial details better. At the same time, the rest part of the scene is not affected obviously.

B. Evaluation of the proposed detail enhancement component

In this section, the proposed detail enhancement component is tested on the top of different MEF algorithms. For each MEF algorithm, the proposed detail enhancement component is evaluated by comparing different selections of γ and ϵ in the equation (19). In the comparison experiments, six sets of LDR images were used to compare the effect of different selections of γ, ϵ and λ.

The first two selections of ϵ and λ are 10^{-4}, 0.5 and 2, 0.5. One more selection of ϵ and λ (10^{-4}, 0.03125) recommended

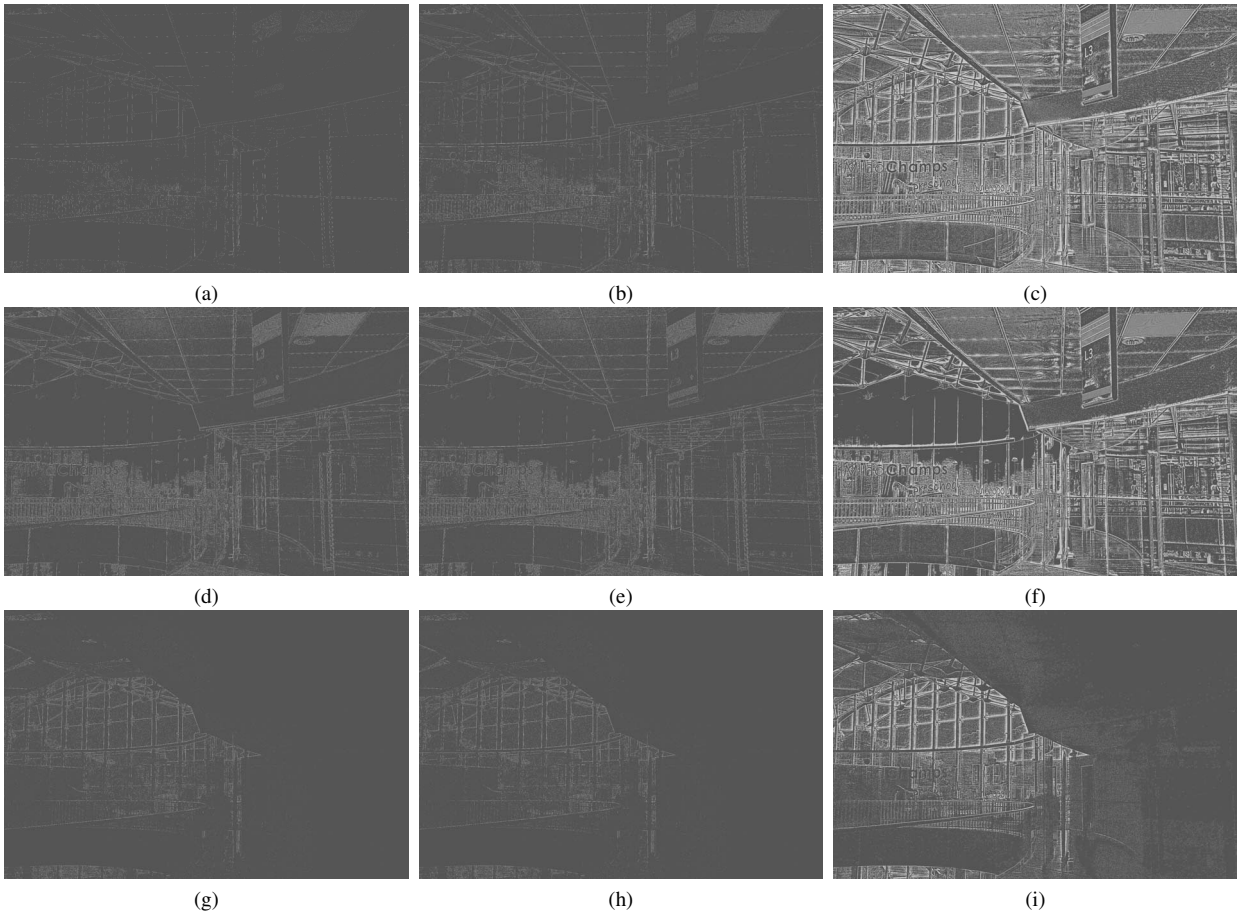

Fig. 11: Comparison of details extracted by different settings for the detail extraction component in [33]. (a), (d) and (g): final extracted detail layer, detail layer of lightest and darkest LDR images for setting $\lambda^{'} = 0.0001, \theta = 0.3$. (d), (e) and (h): setting $\lambda^{'} = 0.0001, \theta = 0.5$. (c), (f) and (i): setting $\lambda^{'} = 0.01, \theta = 1.375$.

TABLE I: MEF-SSIM scores of different algorithms.

LDR sets	[25]	[12]	[22]	[31]	proposed
Treeunil	0.9083	0.9500	**0.9613**	0.9590	0.9606
Tower	0.9810	0.9860	0.9892	**0.9899**	0.9893
Sportcenter	0.9765	0.9710	0.9732	**0.9788**	0.9784
Mask	0.9838	**0.9922**	0.9894	0.9883	0.9910
Lady4	0.9918	**0.9970**	0.9960	0.9958	0.9961
Lady1	0.9805	0.9880	**0.9922**	0.9909	0.9914
Tree	**0.9887**	0.9800	0.9836	0.9817	0.9830
Streetlight	0.9821	0.9830	0.9837	0.9856	**0.9862**
Preschool	0.9840	0.9901	0.9913	**0.9921**	0.9908
Seveneleven	0.9689	0.9691	**0.9785**	0.9725	0.9720
Cafe	0.9575	0.9820	0.9840	0.9830	**0.9847**
Venice	0.9514	0.9661	0.9570	0.9512	**0.9631**
Cemetery Tree	0.9793	0.9855	**0.9890**	0.9875	0.9865
BelgiumHouse	0.9571	0.9740	0.9775	0.9764	**0.9783**
Slide	0.9749	0.9797	0.9827	0.9811	**0.9831**
Sunrise	0.9855	0.9934	**0.9962**	0.9958	0.9946
average	0.9734	0.9804	0.9823	0.9817	**0.9831**

TABLE II: Computation time of 5 MEF algorithms (seconds)

Image Size	[25]	[12]	[22]	[31]	proposed
512*341*3	0.1292	0.0915	0.1496	0.1085	0.1026
795*530*3	0.2778	0.2060	0.3496	0.2405	0.2085
1200*800*3	0.6037	0.5300	0.8987	0.5731	0.4678
2144*1424*3	2.0666	1.7889	3.4092	2.1058	1.7399
4288*2848*3	8.8248	7.6243	15.2065	9.2475	7.8910

in [21] is tested on the proposed MEF algorithm. Correspondingly, the value of γ in the equation (19) is fixed at 0.75. The MEF-SSIM scores of six sets of LDR images are listed in Table III. It is clear that the MEF-SSIM drops significantly with the selections of ϵ and λ being 10^{-4} and 0.5. However, compared with the MEF-SSIM of the proposed exposure fusion, the MEF-SSIM increases slightly with selections of ϵ and λ being 2 and 0.5. In other words, the proposed detail extraction component can be used to improve the MEF-SSIM value even though the extracted fine details are visible. New parameter settings avoid improper selection of fine details. As a result, detail lost in the fusion process is made up while much fewer noises are amplified in this process. Such an improvement can be detected quantitatively as shown in Table III. The corresponding extracted detail layers are posted in Fig. 9.

Different settings are then compared based on the MEF algorithm in [21]. Both the MEF-SSIM and the extracted details are adopted to compare these settings. It is shown in the Table IV that the recommended settings can be adopted to improve the MEF-SSIM for the multi-scale exposure fusion algorithm in [21]. It is demonstrated in Fig. 10 that the extracted details

TABLE III: MEF-SSIM of three different settings of ϵ, λ based on the proposed MEF algorithm.

set \ $[\epsilon, \lambda]$	proposed MEF	[21]	$[10^{-4}, 0.5]$	$[2, 0.5]$
SevenEleven	**0.9720**	0.9719	0.9713	**0.9720**
preschool	0.9908	0.9907	0.9863	**0.9909**
tower	0.9893	**0.9895**	0.9850	**0.9894**
treeunil	0.9606	**0.9607**	0.9596	**0.9607**
BelgiumHouse	**0.9783**	**0.9783**	0.9780	**0.9783**
sportscenter	0.9784	**0.9786**	0.9783	**0.9786**
average	0.9782	**0.9783**	0.9764	**0.9783**
rank	3	2	4	1

are visible by the proposed settings and the settings of ϵ and λ as 10^{-4} and 0.5. Therefore, the proposed settings can also be adopted to improve the MEF-SSIM and to extract visible details for the multi-scale exposure fusion algorithm in [21]. This indicates that it is important to exclude noise from the detail layer for detail enhancement of multi-scale exposure fusion algorithms. A similar testing is performed on the MEF [33] and the detail extraction component in [33]. Three groups of settings of parameters $\lambda^{'}, \theta$ are tested based on the MEF in [33]. In Table V, $\lambda^{'}$ is a regularization coefficient in the cost function, recommended as 0.01, in [33] similar to the λ in equation (18). In [33], extracted detail layer is added to the intermediate fusion image. The coefficient of that detail layer is θ, recommended as 1.375 in [33]. The same conclusion can be obtained from Table V and Fig. 11. Therefore, the proposed detail enhancement component is indeed able to improve the MEF-SSIM values when visible fine details are added to intermediate fused images.

TABLE IV: MEF-SSIM of three different settings of ϵ, λ based on the MEF algorithm in [21].

set	MEF [21]	[21]	ϵ,$\lambda = 10^{-4}$,0.5	proposed
SevenEleven	0.9779	0.9742	0.9743	**0.9780**
preschool	**0.9903**	0.9892	0.9825	0.9891
tower	**0.9893**	0.9892	0.9835	0.9892
treeunil	0.9561	0.9573	0.9576	**0.9583**
BelgiumHouse	0.9762	0.9767	0.9733	**0.9770**
sportscenter	0.9742	0.9742	0.9708	**0.9743**
average	0.9773	0.9768	0.9737	**0.9777**
rank	2	3	4	1

TABLE V: MEF-SSIM of three different settings of $\lambda^{'}, \theta$ based on the MEF algorithm in [33].

set \ $\lambda^{'}, \theta$	MEF [33]	0.01, 1.375	10^{-4}, 0.5	10^{-4}, 0.3
SevenEleven	**0.9785**	0.9282	0.9783	**0.9785**
preschool	**0.9913**	0.9282	0.9911	0.9912
tower	0.9892	0.9404	0.9891	**0.9893**
treeunil	0.9613	0.9452	**0.9615**	**0.9615**
BelgiumHouse	0.9775	0.9374	**0.9776**	**0.9776**
sportscenter	**0.9732**	0.9555	0.9731	**0.9732**
average	0.9785	0.9392	0.9785	**0.9786**

V. Conclusion

A simpler multi-scale exposure fusion algorithm has been introduced to fuse differently exposed images in the YUV color space in this paper. With the new weighting in YUV color space and the efficient implementation of smoothing pyramids, the proposed algorithm can preserve details in the brightest and darkest regions of high dynamic range scenes with low noise and color distortion. Both qualitative and quantitative evaluations illustrate that the proposed algorithm can produce comparable or even better fusion results while significantly reducing the computational complexity. Thus, the proposed fusion algorithm is friendlier to the smartphones than the state-of-the-art multi-scale exposure fusion algorithms which are based on edge-preserving smoothing filters. In addition, a simple detail enhancement algorithm is proposed for the multi-scale exposure fusion algorithm. The proposed detail enhancement component can be used to produce images with higher MEF-SSIM values and visible fine details. The component is thus very attractive for PC based applications.

References

[1] P. E. Debevec and J. Malik, "Recovering high dynamic range radiance maps from photographs," in *Proceedings of the 24th annual conference on Computer graphics and interactive techniques*. ACM Press/Addison-Wesley Publishing Co., May 1997, pp. 369–378.

[2] F. Durand and J. Dorsey, "Fast bilateral filtering for the display of high-dynamic-range images," *SIGGRAPH*, pp. 257–266, Aug 2002.

[3] Z. Farbman, R.Fattal, D.Lischinshi, and R.Szeliski, "Edge-preserving decompostions for multi-scale tone and details manipulation," *ACM Trans. Graph*, vol. 27, pp. 249–256, Aug 2008.

[4] Z. Li and J. Zheng, "Visual-salience-based tone mapping for high dynamic range images," *IEEE Transactions on Industrial Electronics*, vol. 61, no. 12, pp. 7076–7082, Dec 2014.

[5] G. Eilertsen, R. Wanat, R. K. Mantiuk, and J. Unger, "Evaluation of tone mapping operators for hdr-video," in *Computer Graphics Forum*. Wiley Online Library, October 2013, vol. 32, pp. 275–284.

[6] A. Abd el kader, H. El-Din Moustafa, and S. Rehan, "Performance measures for image fusion based on wavelet transform and curvelet transform," in *2011 28th National Radio Science Conference (NRSC)*, April 2011, pp. 1–7.

[7] Jianbo Xu, Youjun Huang, and Jianli Wang, "Multi-exposure images of wavelet transform fusion," in *International Conference on Digital Image Processing*, 2013, pp. –.

[8] Mingjing Li and Yubing Dong, "Review of image fusion algorithm based on multiscale decomposition," in *Proceedings 2013 International Conference on Mechatronic Sciences, Electric Engineering and Computer (MEC)*, Dec 2013, pp. 1422–1425.

[9] I. Merianos and N. Mitianoudis, "A hybrid multiple exposure image fusion approach for hdr image synthesis," in *2016 IEEE International Conference on Imaging Systems and Techniques (IST)*, Oct 2016, pp. 222–226.

[10] M. Nejati, M. Karimi, S. M. R. Soroushmehr, N. Karimi, S. Samavi, and K. Najarian, "Fast exposure fusion using exposedness function," in *2017 IEEE International Conference on Image Processing (ICIP)*, Sept 2017, pp. 2234–2238.

[11] Tomislav Kartalov and Zoran Ivanovski, "High quality exposure fusion for mobile platforms," in *IEEE Eurocon 2017 - International Conference on Smart Technologies*, 2017, pp. 297–300.

[12] T. Mertens, J. Kautz, and F. V. Reeth, "Exposure fusion," in *Computer Graphics and Applications, 2007. PG '07. 15th Pacific Conference on*, Oct 2007, pp. 382–390.

[13] A. Ardeshir Goshtasby and Stavri Nikolov, "Guest editorial: Image fusion: Advances in the state of the art," *Inf. Fusion*, vol. 8, no. 2, pp. 114–118, Apr. 2007.

[14] P. Burt and E. Adelson, "The laplacian pyramid as a compact image code," *IEEE Transactions on Communications*, vol. 31, no. 4, pp. 532–540, Apr 1983.

[15] K. Ma, K. Zeng, and Z. Wang, "Perceptual quality assessment for multi-exposure image fusion," *IEEE Transactions on Image Processing*, vol. 24, no. 11, pp. 3345–3356, Nov 2015.

[16] C. Tomasi and R. Manduchi, "Bilateral filtering for gray and color images," in *Sixth International Conference on Computer Vision (IEEE Cat. No.98CH36271)*, Jan 1998, pp. 839–846.

[17] K. He, J. Sun, and X. Tang, "Guided image filtering," *IEEE Transactions on Pattern Analysis and Machine Intelligence*, vol. 35, no. 6, pp. 1397–1409, June 2013.

[18] Z. Li, J. Zheng, Z. Zhu, W. Yao, and S. Wu, "Weighted guided image filtering," *IEEE Transactions on Image Processing*, vol. 24, no. 1, pp. 120–129, Jan 2015.

[19] F. Kou, W. Chen, C. Wen, and Z. Li, "Gradient domain guided image filtering," *IEEE Transactions on Image Processing*, vol. 24, no. 11, pp. 4528–4539, Nov 2015.

[20] S. Li, X. Kang, and J. Hu, "Image fusion with guided filtering," *IEEE Transactions on Image Processing*, vol. 22, no. 7, pp. 2864–2875, July 2013.

[21] Z. Li, Z. Wei, C. Wen, and J. Zheng, "Detail-enhanced multi-scale exposure fusion," *IEEE Transactions on Image Processing*, vol. 26, no. 3, pp. 1243–1252, March 2017.

[22] F. Kou, Z. Li, C. Wen, and W. Chen, "Multi-scale exposure fusion via gradient domain guided image filtering," in *2017 IEEE International Conference on Multimedia and Expo (ICME)*, July 2017, pp. 1105–1110.

[23] J. Cai, S. Gu, L. Zhang, and L. Zhang, "Learning a deep single image contrast enhancer from multi-exposure images," *IEEE Transactions on Image Processing*, vol. PP, no. 99, pp. 1–1, Jan 2018.

[24] Y. Liu, D. Wang, J. Zhang, and X. Chen, "A fast fusion method for multi-exposure image in yuv color space," in *2018 IEEE 3rd Advanced Information Technology, Electronic and Automation Control Conference (IAEAC)*, Oct 2018, pp. 1685–1689.

[25] C. O. Ancuti, C. Ancuti, C. De Vleeschouwer, and A. C. Bovik, "Single-scale fusion: An effective approach to merging images," *IEEE Transactions on Image Processing*, vol. 26, no. 1, pp. 65–78, Jan 2017.

[26] R. Shen, I. Cheng, J. Shi, and A. Basu, "Generalized random walks for fusion of multi-exposure images," *IEEE Transactions on Image Processing*, vol. 20, no. 12, pp. 3634–3646, Dec 2011.

[27] M. Song, D. Tao, C. Chen, J. Bu, J. Luo, and C. Zhang, "Probabilistic exposure fusion," *IEEE Transactions on Image Processing*, vol. 21, no. 1, pp. 341–357, Jan 2012.

[28] Z. G. Li, J. H. Zheng, and S. Rahardja, "Detail-enhanced exposure fusion," *IEEE Transactions on Image Processing*, vol. 21, no. 11, pp. 4672–4676, Nov 2012.

[29] S. Di Zenzo, "A note on the gradient of a multi-image," *Comp.vis.graph.im.proc*, vol. 33, no. 1, pp. 116–125, 1986.

[30] F. Kou, W. Chen, X. Wu, and Z. Li, "Intelligent detail enhancement for differently exposed images," in *2017 IEEE International Conference on Image Processing (ICIP)*, Sept 2017, pp. 3185–3189.

[31] Fei Kou, Zhengguo Li, Changyun Wen, and Weihai Chen, "Edge-preserving smoothing pyramid based multi-scale exposure fusion," *Journal of Visual Communication and Image Representation*, vol. 53, pp. 235–244, 2018.

[32] Q. Wang, W. Chen, X. Wu, and Z. Li, "Detail preserving multi-scale exposure fusion," in *2018 25th IEEE International Conference on Image Processing (ICIP)*, Oct 2018, pp. 1713–1717.

[33] F. Kou, Z. Wei, W. Chen, X. Wu, C. Wen, and Z. Li, "Intelligent detail enhancement for exposure fusion," *IEEE Transactions on Multimedia*, vol. 20, no. 2, pp. 484–495, Feb 2018.

[34] C. F. Hall and E. L. Hall, "A nonlinear model for the spatial characteristics of the human visual system," *IEEE Transactions on Systems, Man, and Cybernetics*, vol. 7, no. 3, pp. 161–170, March 1977.

[35] D. Min, S. Choi, J. Lu, B. Ham, K. Sohn, and M. N. Do, "Fast global image smoothing based on weighted least squares," *IEEE Transactions on Image Processing*, vol. 23, no. 12, pp. 5638–5653, Dec 2014.